Effects of pressurization and surface tension on drawing Ge-Sb-Se chalcogenide glass suspended-core fiber

Wu, Shengling; Fleming, Simon; Kuhlmey, Boris T.; Ebendorff-Heidepriem, Heike; Stefani, Alessio

Published in:
Optical Materials Express

Link to article, DOI:
10.1364/OME.9.001933

Publication date:
2019

Document Version
Publisher's PDF, also known as Version of record

Research Article Vol. 9, No. 4 / 1 April 2019 / Optical Materials Express 1933
Optical Materials EXPRESS

Effects of pressurization and surface tension on drawing Ge-Sb-Se chalcogenide glass suspended-core fiber

WU SHENGLING,[1,*] SIMON FLEMING,[1] BORIS T. KUHLMEY,[1] HEIKE EBENDORFF-HEIDEPRIEM,[2] AND ALESSIO STEFANI[1,3]

[1] *Institute of Photonics and Optical Science (IPOS), School of Physics, The University of Sydney, NSW 2006, Australia*
[2] *Institute for Photonics and Advanced Sensing (IPAS),University of Adelaide, SA 5005, Australia*
[3] *DTU Fotonik, Department of Photonics Engineering, Technical University of Denmark, DK-2800 Kgs. Lyngby, Denmark*
[*] *shengling.wu@sydney.edu.au*

Abstract: Drawing chalcogenide glass microstructured optical fibers efficiently requires a good understanding of the different drawing conditions beforehand, due to the high cost of the chalcogenide glass materials. A simulation based on Stokes' model that includes pressurization and glass surface tension is validated with respect to drawing a $Ge_{28}Sb_{12}Se_{60}$ chalcogenide glass single hole capillary, as well as microstructured optical fiber with three holes, with different pressurizations. Suspended-core $Ge_{28}Sb_{12}Se_{60}$ fibers with bridges just hundreds of nanometer wide are drawn using parameters predicted by the simulations. These fibers should be suitable for applications such as generating mid-infrared (MIR) supercontinuum based on chalcogenide glasses.

1. Introduction

Microstructured optical fibers (MOFs), and specifically suspended-core optical fibers, based on chalcogenide glasses have been studied intensively due to their great potential for applications to nonlinear optical devices. The small central core structure provides tight confinement of light, and high nonlinearity [1]. Combined with chalcogenide glasses, which have high transmission in the infrared region (up to 20 μm), and large nonlinearity (1000 times that of silica) [2], suspended-core fibers have been used to realize cascaded Raman shifts [3], highly efficient four-wave mixing [4] and especially to generate supercontinuum in the mid-infrared region [5,6]. One of the most important advantages of suspended-core fiber to be used for generating supercontinuum is that it can shift the zero-dispersion wavelength to shorter values, permitting pumping by a commercially available laser source [7,8]. To achieve this, a suitable geometry with small suspended-core size and thin bridges is required. Conventional fabrication methods such as extrusion [9], ultrasonic drilling [10], casting [11], or stack-and-draw [12] have been used to produce suspended-core fiber preforms. Normally, pressurization is introduced in the final step of the fiber drawing process to expand hole sizes and reduce bridge thicknesses. Inevitably, a certain amount of empirical 'trial and error' is necessary to determine the amount of required pressurization. However, the high cost and limited availability of the chalcogenide glasses provides strong motivation to investigate the dynamics of the viscous glass during the drawing process before starting fabrication.

Some mathematical analyses have been performed to investigate the drawing conditions from capillaries to MOFs. In 2002, A. D. Fitt introduced a theoretical model for drawing single hole capillaries and included both effects of surface tension at the hole glass interface and inner pressurization, for a steady-state drawing process [13], which has subsequently been improved

#359286 https://doi.org/10.1364/OME.9.001933
Journal © 2019 Received 8 Feb 2019; revised 21 Mar 2019; accepted 21 Mar 2019; published 27 Mar 2019

Optical Materials EXPRESS

and simplified by other researchers [14–16]. Recently, this model has been successfully applied to predicting the experimental drawing parameters to obtain silica MOF with rotationally symmetric multi-hole structure. However, for asymmetric structures, Fitt's model is unable to predict the final structure of the MOF, since it does not take into account the surface tension effects of the material outside the structure [17]. Y. M. Stokes described a mathematical model of drawing MOF for arbitrary cross-sectional profiles, based on the fiber drawing tension [18], and M. J. Chen demonstrated this model can be used to predict the fiber geometry from tubular preform successfully, when active channel pressurization has been introduced [19].

In this paper, we use and experimentally validate Stokes' model for drawing $Ge_{28}Sb_{12}Se_{60}$ chalcogenide glass suspended-core fibers. Using the stack-and-draw method and insight from this model, chalcogenide glass suspended-core fibers with required structure were obtained, with potential to be used for supercontinuum generation in the mid-infrared region.

2. Stokes' mathematical model with active pressurization

Starting from the tubular preform, the Stokes' model presents the evolution of the ratio of the inner and the outer radii from the preform, ρ_0, to the tubular fiber, ρ_L. Here the subscript '0' and 'L' represent the preform and the fiber respectively, so $\rho_0 = r_0/R_0$ and $\rho_L = r_L/R_L$, where R and r are the radius of outer and inner diameters of the preform or the fiber. An additional parameter α has been introduced to describe the geometry of the preform and the fiber for mathematical convenience, defined as [18,19]:

$$\alpha_0 = \alpha(\rho_0), \quad \alpha_L = \alpha(\rho_L), \quad \text{where } \alpha(\rho) = \frac{1}{\sqrt{\pi}}\sqrt{\frac{1-\rho}{1+\rho}}. \tag{1}$$

In practice, we are more interested in the ratio of inner and outer radius of the fiber after the drawing process, so this ratio ρ_L can be obtained by the rearrangement of (1):

$$\rho_L = \frac{1-\pi\alpha_L^2}{1+\pi\alpha_L^2}. \tag{2}$$

For the case of drawing tubular fibers with pressurization, the fiber geometry α_L can be obtained from Stokes' model by solving the following system of differential equations:

$$\frac{d\alpha}{d\tau} = \frac{1}{2} - \frac{1}{8\pi\alpha}(1-\pi^2\alpha^4)\mathscr{P}\chi, \tag{3}$$

$$\frac{d\chi}{d\tau} = \frac{1}{6}\frac{\chi}{\alpha} - \mathscr{T}, \tag{4}$$

where τ is the 'reduced time', which measures the time from the beginning of the deformation ($\tau = 0$), to its end ($\tau = \tau_L$), along the neck-down region at $x = 0$ and $x = L$. L is the length of the neck-down region, and within this region the temperature of the fiber is assumed not to vary significantly, as shown in Fig. 1(a), therefore a constant value of temperature is used in the simulations. $\chi = \sqrt{A/A_0}$ is the square root of the scaled cross-section area, which evolves from the preform ($\chi = 1$) to the fiber ($\chi = \sqrt{A_L/A_0} = 1/\sqrt{D}$), $D = U_d/U_f$, where D is the drawing ratio, U_d is the drawing speed, and U_f is the feeding speed. A_L and A_0 are the cross-sectional area of the preform and fiber excluding the air fraction, thus

$$A_0 = \pi R_0^2(1-\rho_0^2), \quad A_L = \pi R_L^2(1-\rho_L^2) \tag{5}$$

Optical Materials EXPRESS

$\mathscr{P}$ and $\mathscr{T}$ are dimensionless parameters of the active pressurization and the fiber drawing tension, and they are related to the real active pressurization P and fiber drawing tension σ by

$$\sigma = 6\gamma\sqrt{A_0}\mathscr{T}, \tag{6}$$

$$P = \frac{\gamma}{\sqrt{A_0}}\mathscr{P}, \tag{7}$$

where γ is the surface tension. Thus, once the reduced time τ_L is determined, the final fiber geometry α_L can be obtained by solving the differential equations (3)-(4) numerically. τ_L can be calculated from the following equation:

$$\left[\sqrt{D}\left(\frac{\tau_L}{2\alpha_0}+1\right)^{1/3}\right]^{-1} + \left(\frac{\mathscr{R}}{3M\alpha_0}\right)^{-1}\left[\left(\frac{\tau_L}{2\alpha_0}+1\right)^{2/3}-1\right]\log\left[\sqrt{D}\left(\frac{\tau_L}{2\alpha_0}+1\right)^{1/3}\right] = 1, \tag{8}$$

where $\mathscr{R} = \gamma L/(\mu U_f\sqrt{A_0})$ is the dimensionless surface tension, and M is the inverse harmonic mean of the glass viscosity μ over the neck-down region. More details can be found in [18]. With a set of known initial drawing conditions, namely the geometry of the preform α_0, the drawing ratio D, the surface tension of the glass γ, the glass viscosity μ, and the fiber drawing tension σ, which can be measured during drawing, the reduced time τ_L can be calculated directly, and the final fiber geometry $\alpha(\tau_L)$ retrieved numerically from (3)-(4).

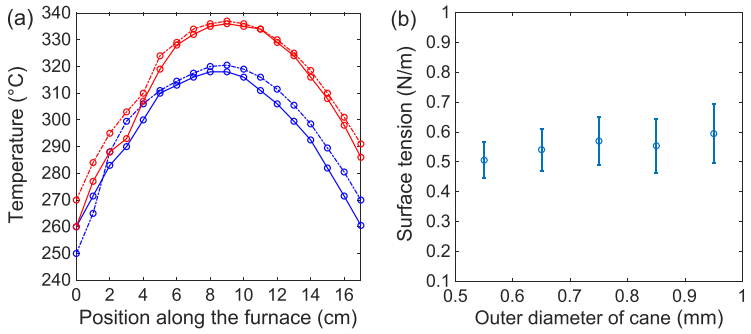

Fig. 1. (a) Temperature profile of the glass preform (solid line), and at the center of the furnace (dotted line), when the furnace temperature was set to be 325 °C (blue) and 345 °C (red) as a function of the position along the furnace. (b) Results of the surface tension measurements with IG5 glass rods of various sizes.

Knowing the fiber drawing tension is necessary to compare the experiments and the simulations. Effectively, when doing the simulations, the drawing tension can be estimated by knowing the set temperature and the viscosity of the material via the following relationship [20]:

$$\sigma = -\frac{6\pi U_f r^{*2}\mu\ln(\sqrt{U_f/U_d})}{L}, \tag{9}$$

where r^* is the effective radius of the fiber, which is calculated from the cross-section of the fiber excluding the air fraction, and again L is the length of the neck-down region (in our case 3 cm, as measured over several drawing trials).

3. Material and facility related parameters

To use Stokes' models for simulating the effects of surface tension and inner hole pressurization, several parameters of the selected material need to be known in advance: the viscosity-temperature relationship and the surface tension of the material. Here we chose $Ge_{28}Sb_{12}Se_{60}$ chalcogenide glass (IG5, IRradiance Glass Inc.), which has a high transmission up to 12 μm and high material nonlinearity [21], and is the only commercially available arsenic-free chalcogenide glass.

Optical Materials EXPRESS

3.1. Temperature dependence of viscosity

To calculate the viscosity of the glass at the set temperature, a two-parameter Arrhenius equation can be used [22]. For IG5 glass, the glass transition temperature (T_g) and softening temperature are 285 °C and 348 °C [23], where the viscosities at these two temperatures are 10^{12} Pa.s and $10^{6.6}$ Pa.s respectively. Introducing these two groups of viscosity-temperature values into the equation, an empirical viscosity-temperature relationship can be obtained:

$$\log \mu = -41.2 + 29702/(T + 273.15). \tag{10}$$

where T is the temperature in degree Celsius. The accuracy of this relationship relies on the exact values of these two temperatures. However, there is a few degrees uncertainty on both of them. This translates into a large potential viscosity error range for temperatures far from those used for the fit. Our simulations are mostly performed at a temperature of 345 °C, therefore the error in viscosity is limited and it is anyway taken into account in the calculations.

3.2. Temperature profile along the furnace

The fiber drawing process is normally performed in a furnace. The temperature of the preform may be different to the temperature of the furnace, and sometimes this difference can be up to several hundreds degrees when drawing silica fibers [17]. To determine the temperature of the IG5 glass preform, a thermocouple was inserted into (and in thermal contact with) an IG5 glass sealed tube with outer diameter of 5 mm, and fed slowly into the furnace. The furnace used here has a 4 cm diameter, 30 cm long heating coil, and is operated in a standard laboratory environment, and without gas purging. The IG5 glass drawing temperature region for our experiments is between 325 °C and 345 °C, which we determined by drawing successfully a range of IG5 glass preforms with outer diameters from 1 to 10 mm. Thus the measurements were performed with furnace setting temperature at 325 °C and 345 °C. The temperature profile of the center of the furnace was also measured with this same procedure but without the IG5 glass tube for comparison. Each data point was recorded after reaching thermal equilibrium, which took about three minutes and temperature stability was ensured by monitoring over a further two minutes.

Figure 1(a) shows the temperature profile within the glass preform (solid line) and in the center of the furnace (dotted line) along the furnace length, for temperature setting of 325 °C (blue) and 345 °C (red). The temperature profile in the glass is very close to that of the furnace without the glass for the drawing temperature region. The temperature profile might change slightly for the preforms of different sizes, because the heat absorption efficiency is dependent on the preform size [20]. Since it is impractical to measure the temperature profile on the glass preform for each drawing situation, and the temperature within the neck-down region does not change significantly, in the following simulations the temperature as measured in Fig. 1(a) (scaled to the maximum and constant temperature when required) is used.

3.3. Surface tension

The surface tension of IG5 glass can be measured with the elongation technique [24], and simplified here by using the drawing furnace instead of a CO_2 laser as the heating source. The bottom of an IG5 glass cane with a radius r was positioned in the furnace at the location of highest temperature, and it was fed into the furnace slowly to increase the volume of the heated part. The heated volume is expected to be pulled upwards into a sphere, when the downward weight force is smaller than the upward surface tension force. When these two forces are in equilibrium, the surface tension can be calculated as

$$\gamma = \frac{mg}{\pi r} \tag{11}$$

Optical Materials EXPRESS

where m is the mass of glass hanging below the heated volume, and g is the gravitational acceleration. As the rod is slowly fed into the hot zone it should neck and drop when the weight of the glass below the softened region just exceeds the surface tension. Such technique is chosen because of the narrow length of hot zone of the furnace, and to ensure that enough material is softened while not having extra weight below the hot zone.

An IG5 glass rod with uniform outer diameter was used to measure the surface tension, and the furnace temperature was set to be 380 °C (i.e., viscosity at $10^{4.2\pm0.2}$ Pa.s), to ensure the glass can deform by its own weight. The glass rod was fed into the furnace with a speed of 0.2 mm/min, to increase the downward weight force slowly, until the heated part dropped. The dropped part was collected and then weighed with a digital balance within ±0.1 mg. This process was repeated five times, with different outer diameters varied from 0.55 mm to 0.95 mm. The results are shown in Fig. 1(b), and the mean value is 0.54 ± 0.10 N/m. The relatively large errors are caused by the 1 cm long isothermal region of the 3 cm neck down part in the furnace, so the surface tension errors are calculated from the uncertainty given by the weight of this 1 cm length of the rods. The isothermal region is determined as the length of the hot zone with a temperature difference from the maximum measured temperature within the precision of the thermocouple used for the measurement, i.e. 0.5 °C. Considering this, the weight of the dropped part might be larger than expected, so the surface tension of IG5 glass in practice is unlikely to be in the lower half of the uncertainty range. To check the validity of this method the same experiment was performed with soda-lime glass using exactly the same procedure, at the temperature of 780 °C. The slightly larger result of 0.38 N/m compared to the reference value of 0.31 N/m supports the expectation that slightly larger values for surface tension are obtained with this method [25]. The value is in reasonable agreement with the expected magnitude, and for our simulations we use a value of 0.54 N/m for the surface tension of IG5. Because of the strong sensitivity to surface tension, simulations are also carried out with the extremal values of surface tension within the error range to calculate the error in simulation results.

4. Fabrication methodology

4.1. Microstructured cane

To fabricate the IG5 glass suspended-core fibers, an IG5 glass billet (Fig. 2(a)), was firstly extruded into a tube (Fig. 2(b)) using a specifically designed die. It was pointed out in earlier works that the Ge-Sb-Se chalcogenide glass is difficult to draw and easily crystallizes [26–28]. However, we found that the IG5 glass has a relatively large drawing temperature window, and can be easily drawn from 325 °C to 385 °C without obvious crystallization [29]. This extruded glass tube was then drawn into capillaries (Fig. 2(c)), three of which were selected to be stacked into a triangular arrangement and inserted into a jacketing tube to realize a fiber preform (Fig. 2(d)). The three-holes geometry preform was then drawn with 0.8 bar vacuum applied between the inner tubes and the jacket, to seal the gaps between the capillaries and the outside jacket, into a microstructured cane (Fig. 2(e)). Finally, the microstructured cane was drawn to fiber dimensions with different pressurizations.

4.2. Pressurization procedure

To test the effect of pressurization during drawing and to compare it to the simulated results, two different structures were selected: a single hole capillary and a suspended-core structure. One of the IG5 capillaries was chosen as a preform to draw with different pressurizations. This preform has an inner radius r_0 = 1.4 mm, and outer radius R_0 = 2.3 mm. Feeding and drawing velocity were set to be 1.5 mm/min and 10.5 mm/min respectively, and the introduced pressurization was increased from 60 mbar to 80 mbar with increments of 5 mbar. The pressure range for the experiment was chosen to obtain a significant change in the structure. Each step was drawn for

Optical Materials EXPRESS

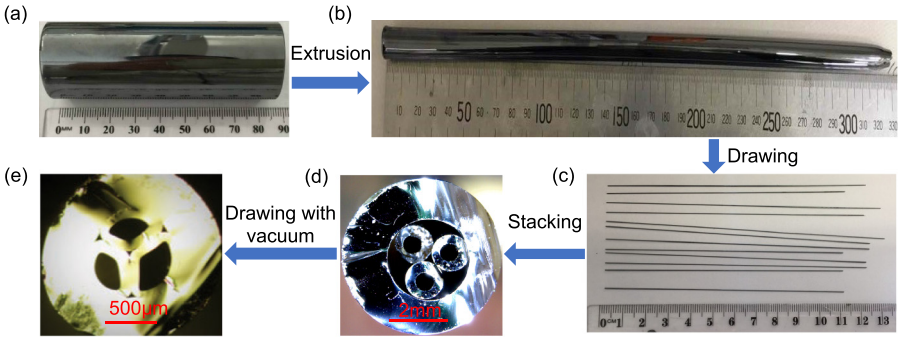

Fig. 2. Process flow chart of fabrication of IG5 microstructured cane: (a) glass billet, (b) extruded tube, (c) glass capillaries, (d) preform, (e) microstructured cane.

10 minutes, to allow the different drawing conditions to stabilize and reflect the steady state. The microstructured cane which is shown in Fig. 2(e) was then used for drawing with the same varied pressurizations, and it has an outer radius $R_0 = 0.8$ mm. Feeding and drawing velocity were 1.5 mm/min and 5.0 mm/min respectively. The increment of pressurizations and the drawing process was the same as for the single capillary.

5. Results and discussion

5.1. Single capillary

Figure 3(a) shows a cross-section image of the IG5 glass capillary drawn without pressurization, and Figs. 3(b) to 3(f) show the cross-section images of drawing with pressurization from 60 mbar to 80 mbar. As expected, the wall became thinner when higher pressurization was applied. Figure 3(g) shows the comparison between the theoretical model and experimental results for the air fraction of the capillary after drawing with different pressurizations, and the experimental air fraction is obtained by measuring the inner and outer diameters of the microscope images. This comparison indicates that Stokes' model can accurately predict the final air fraction of a chalcogenide glass single hole structure drawn with different pressurization. The central values for the simulation are calculated using a surface tension $\gamma = 0.54$ N/m, and the error bars are calculated from simulations, with the upper and lower values of the surface tension (0.44 N/m and 0.64 N/m). The close results validate the IG5 glass surface tension should be close to 0.54 N/m. Note the self-pressurization effect observed by Chen et al [19] was not taken into account in the simulations, since the applied pressurization in our case is much larger than that of the reference (5 mbar to 30 mbar), and the surface tension of IG5 glass is also larger than the material used in the reference (F2 glass, $\gamma = 0.23$ N/m).

5.2. Three-holes structure

The case of drawing the three-holes microstructured cane with pressure is more complex, because the separation of the holes will decrease with the increase of the introduced pressurization, changing the effect of surface tension. The interaction between the inner holes cannot be ignored in this structure. In the limit where the separation between holes becomes small, the three holes can be seen as behaving as one large hole, the hole radius effectively jumping up. At such threshold a small change in pressure will result in a large expansion of the structure as also predicted by Stokes [18]. To analyze the behavior of the holes as separated entities or as a single collective hole, we simulated the drawing process for both the limit at which each hole is independent, and for the limit at which all the holes contribute to a single hollow cavity in fiber.

Optical Materials EXPRESS

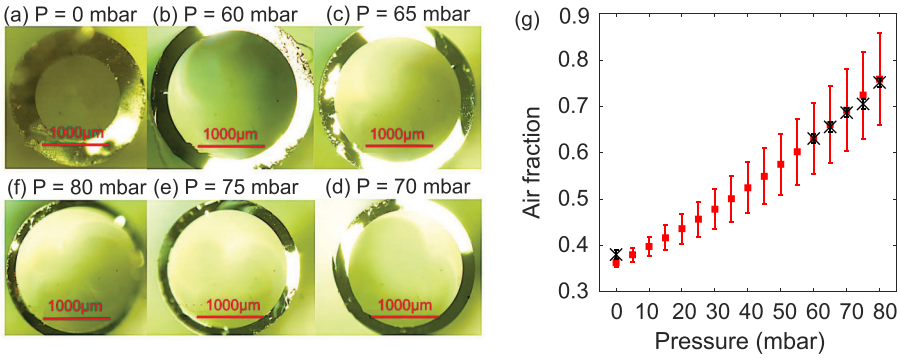

Fig. 3. (a-f) Cross-section microscope images of the capillary when drawn with different pressurizations. (g) Experimental (black crosses) and simulated (red filled squares) air fraction of the capillary when drawn with different pressurizations.

5.2.1. Asymptotic regimes of holes' expansion

The case of the holes acting as separated entities is simulated by assuming there is only one capillary being drawn, which has a glass surrounding corresponding to the the largest circle that can be traced before reaching the other air holes (dashed line circle in Fig. 4(a)). To compare with the experiments, the total air fraction is then calculated from the simulation by multiplying the simulated area of the hollow part of the capillary (Fig. 4(b) to 4(c)) by the number of capillaries (in this case 3) to obtain the total air surface $3A_h$, and dividing it by the total cross-section

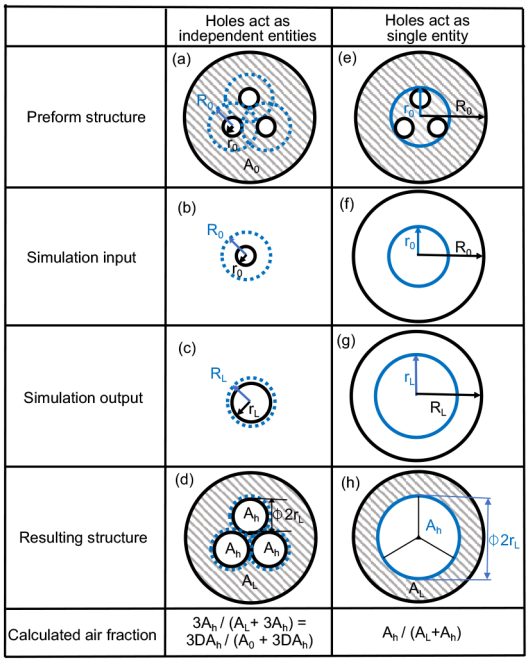

Fig. 4. Schematic diagram of drawing the three-hole cane when holes act as independent entities (a-d) or single entity (e-h) case: (a) and (e) cross-section of the preform, (b) and (f) input parameters of the simulation, (c) and (g) output parameters of the simulation, (d) and (h) resulting structure. D is the drawing ratio.

Optical Materials EXPRESS

area of A_L+3A_h (Fig. 4(d)), where A_L is the scaled (by the drawing ratio) cross-section area of the glass. This is because in this case we treat the holes as independent cavities, the outer diameter of the overall fiber cannot be obtained directly from the simulation. We then look at the holes/microstructure as a one hollow entity, with diameter that of the smallest excircle (which is the smallest circle to completely circumscribe the holes) of the air holes (blue solid circle in Fig. 4(e)), in a tube with same outer diameter as the preform (Fig. 4(f)). The air fraction is calculated as the ratio between the area of the resulting simulated excircle (blue circle in Fig. 4(g)) and that of the overall fiber (A_L+A_h in Fig. 4(h)), which can be obtained from the simulation directly.

5.2.2. Three-hole structure drawing results

Figures 5(a) to 5(f) show the microstructured cane drawn to fiber dimension with different pressurizations. A sudden change in the structure occurred when the introduced pressure was increased from 70 mbar to 75 mbar, which confirmed the existence of a threshold between the two asymptotic regimes. The simulated and experimental results are shown in Fig. 5(g). The blue squares are the simulated air fraction results of $3A_h/(A_L + 3A_h)$, which consider the holes as isolated holes. This case nicely matches the experimental results when the introduced pressurization is below the threshold, i.e. lower than 70 mbar. The red circles are the simulated results when considering the three holes to act as single hole, i.e. $A_h/(A_L+A_h)$. They do not fit the experimental results until the introduced pressure is larger than the threshold, where the fiber begins to form a suspended-core structure.

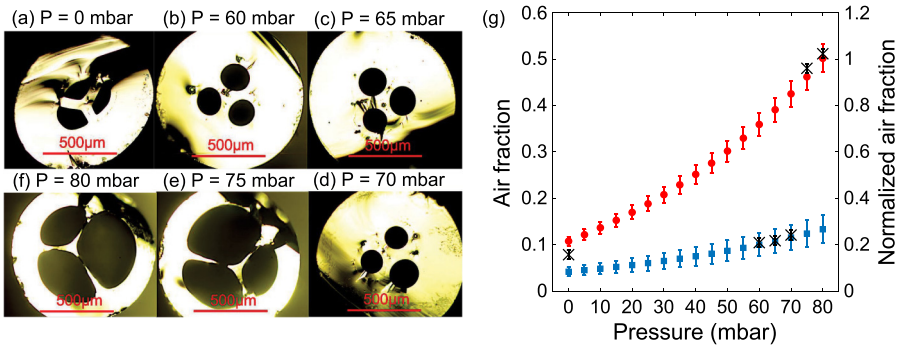

Fig. 5. (a-f) Cross-section microscope images of the MOF when drawn with different pressurizations. (g) Experimental and simulated air fraction of the three-holes cane drawn with different pressurizations. Black crosses: experimental air fraction; blue filled squares: simulated air fraction when considering each hole as independent; red filled circles: simulated air fraction when considering holes acting as a single entity.

5.2.3. Normalized air fraction.

It is clear that these two asymptotic situations are quite different. At first, the evolution of the holes is determined by the separation between holes and not by the jacket dimension. In contrast, when the holes become close and can be treated as a single large hole, the microstructure's evolution is strongly dependent on the jacket's outer dimension. Although we want to gain an understanding of the effect of pressure on the structure, our main goal is to have an indication of the required parameters for the fabrication of a suspended-core fiber. To do that, considering the overall air fraction is not very useful to assess the quality of a suspended-core fiber, as this will change depending on the preform (jacket size, initial capillaries air fraction,. . .). We therefore define a normalized air fraction which excludes the jacket surrounding the capillaries. Doing

Optical Materials EXPRESS

so, we obtain a reference unitary parameter indicating when the fabricated fiber approaches a suspended-core structure. The simulations are still performed considering the fiber dimensions as described above, but the solid component of the air fraction only includes the excircle of the single capillaries glass surrounding. Such excircle is the red solid line circle (C_1) in Fig. 6(a). In terms of the fabrication, it can be approximated that when the excircle of the holes (C_2 in Fig. 6(a), same as in Fig. 4(e)) completely fill this area (normalized air fraction $A_{C_2}/A_{C_1} = 1$), the structure is likely to be the desired one (Fig. 6(b) to 6(c)) as the glass thickness separating the holes tends to zero. This is of course an idealization, but it gives a preform size independent target for the simulations. With the known parameters of the preform, and the help of Stokes' model, it is possible to simulate the normalized fiber air fraction for different introduced pressurization. Certainly, in some cases it is possible to obtain an even better structure with a normalized air fraction greater than 1, however, this critical value of 1 can lead to a suspended-core fiber structure with limited empirical attempts and while avoiding the explosion of the fiber (the pressure leading to explosion can be also obtained with the simulations). In this drawing experiment, the normalized air fraction is 1.1 when the introduced pressure is 80 mbar.

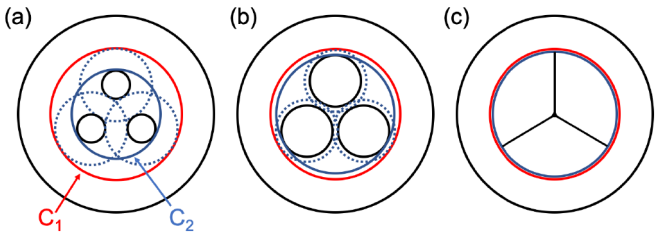

Fig. 6. Schematic of the cross-section when the introduced pressurization is: (a) smaller than the threshold, (b) at about the threshold, (c) larger then the threshold, and the normalized air fraction = 1. C_1 is the normalized excircle, while C_2 is the excircle of the holes.

Overall, the simulations above confirmed our assumptions that the evolution of the holes in MOFs will respond to the introduced pressurization in two stages, due to the existence of a threshold. Though it is difficult to use Stokes' model to predict the threshold precisely and directly, combining it with the normalized air fraction for different pressurization, it revealed a promising fit to the final geometry of IG5 glass suspended-core fibers, which requires large air fraction and thin bridges to support the core. It should be noted that for the desired structures the fiber will always be in the regime where the holes act as a single entity. Therefore, in using the simulations to find the desired drawing parameters, only the simulations with the holes behaving as one collective entity are performed.

5.3. Suspended-core fibers

Using these simulations as described above, we are able to predict the final normalized air fraction of the fiber when drawn with different drawing conditions, facilitating the selection of suitable drawing parameters for different required geometries. Two IG5 glass suspended core fibers with thick and thin jacket have been successfully fabricated, as shown in Fig. 7(a) and 7(b), by introducing a suitable pressurization to expand the normalized air fraction to be around 1 in the final fiber structure. A summary of the parameters used and the drawing results for these two fibers, as well as the normalized air fractions are reported in Table 1. The bridge thicknesses have been reduced to hundreds of nanometers, permitting a very good confinement of light.

The dispersion of the IG5 suspended core fiber with different core diameters d was calculated with the CUDOS MOF Utilities software [30], based on the refractive index values from IRradiance [21]. With the core size of 2 μm (d = 2 μm), these suspended core fibers can greatly shift the zero dispersion wavelength from that of the IG5 material (6.2 μm) to 1.9 μm, as shown

Optical Materials EXPRESS

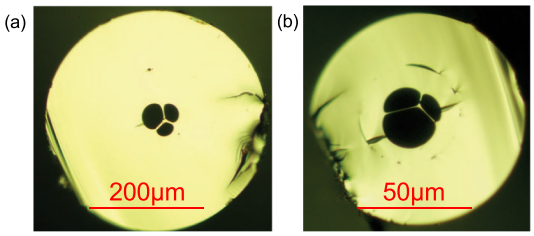

Fig. 7. Optical microscope images of different IG5 glass suspended-core fibers' cross sections.

Table 1. Parameters for the fabrication of IG5 glass suspended-core fibers

Fiber	D	P (mbar)	T(°C)	C_2 (MD, μm)	C_2 (CD, μm)	MN	SN
Fiber (a)	4.0	80	345	79	76	0.88	0.95
Fiber (b)	6.0	90	350	48	45	1.09	0.96

Note: D-drawing ratio, P-introduced pressurization, T-furnace setting temperature, MD-measured diameter, CD-calculated diameter, MN-measured normalized air fraction, SN- simulated normalized air fraction.

in Fig. 8(a) and 8(b). In addition, the fundamental mode can be well confined in the small core, as IG5 glass has large refractive index. The fundamental mode of a 1 μm diameter core is well confined up to 3 μm wavelength, and that of a 2 μm diameter is confined up to 6 μm wavelength. The strong confinement, suitable dispersion and high nonlinearity show a great potential for generating supercontinuum in the MIR with commercial sources.

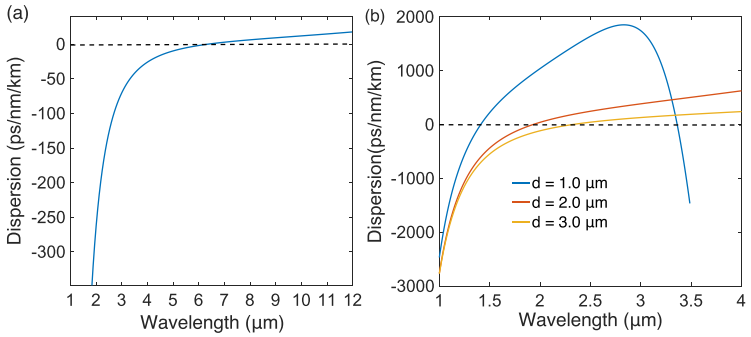

Fig. 8. (a) IG5 glass materials dispersion, (b) the simulated fundamental mode dispersion with different core diameters d of IG5 glass suspended-core fibers.

6. Conclusion

An asymptotic simulation including the effects of pressurization and surface tension in the fiber drawing process based on Stokes' models has been applied to drawing $Ge_{28}Sb_{12}Se_{60}$ (IG5) chalcogenide glass suspended-core fibers. The experimental results of drawing IG5 glass single hole capillary with different pressurizations show a very good agreement with the simulations. A comparison between experimental and simulated results of drawing IG5 glass microstructured cane with three holes at different pressurizations was performed. This comparison confirmed the presence of a threshold pressure at which a large sudden change of the geometry occurs. For pressures lower than the threshold, the inner holes act as isolated entities, while above it they act as a single hole. By introducing a normalized air fraction, which is set to be equal to 1 for a suspended-core like structure, Stokes' model is a useful tool to predict the suitable introduced

Optical Materials EXPRESS

pressurization in the fiber drawing process, to obtain MOFs with required structure. Two different IG5 chalcogenide glass suspended-core fibers have been fabricated successfully by targeting a normalized air fraction around 1. With core sizes as small as 2 μm and with thin bridges, the IG5 glass suspended-core fibers show great potential in nonlinear optical applications especially for generating MIR supercontinuum with commercial laser sources.

Funding

China Scholarship Council (CSC) (201506240031); H2020 Marie Skłodowska-Curie Actions (MSCA) (708860); ANFF Opotfab; Australian Research Council (ARC) (DP140104116).

Acknowledgments

We thank Richard Lwin and Juliano G. Hayashi for providing technical assistance in IG5 glass fiber drawing processes, and Alson Ng from the University of Adelaide for assistance with extrusion.

References

1. K. M. Mohsin, M. S. Alam, D. M. N. Hasan, and M. N. Hossain, "Dispersion and nonlinearity properties of a chalcogenide As_2Se_3 suspended core fiber," Appl. Opt. **50**(25), E102–E107 (2011).
2. J. Troles, L. Brilland, P. Toupin, Q. Coulombier, S. D. Le, D. M. Nguyen, M. Thual, T. Chartier, G. Renversez, D. Mechin, and J. L. Adam, "Chalcogenide suspended-core fibers: Manufacturing and non-linear properties at 1.55 μm," in *2011 13th International Conference on Transparent Optical Networks*, (2011), pp. 1–4.
3. M. Duhant, W. Renard, G. Canat, T. N. Nguyen, F. Smektala, J. Troles, Q. Coulombier, P. Toupin, L. Brilland, P. Bourdon, and G. Renversez, "Fourth-order cascaded Raman shift in AsSe chalcogenide suspended-core fiber pumped at 2 μm," Opt. Lett. **36**(15), 2859–2861 (2011).
4. S. D. Le, D. M. Nguyen, M. Thual, L. Bramerie, M. C. e Silva, K. Lenglé, M. Gay, T. Chartier, L. Brilland, D. Méchin, P. Toupin, and J. Troles, "Efficient four-wave mixing in an ultra-highly nonlinear suspended-core chalcogenide $As_{38}Se_{62}$ fiber," Opt. Express **19**(26), B653–B660 (2011).
5. W. Gao, M. El Amraoui, M. Liao, H. Kawashima, Z. Duan, D. Deng, T. Cheng, T. Suzuki, Y. Messaddeq, and Y. Ohishi, "Mid-infrared supercontinuum generation in a suspended-core As_2S_3 chalcogenide microstructured optical fiber," Opt. Express **21**(8), 9573–9583 (2013).
6. U. Møller, Y. Yu, I. Kubat, C. R. Petersen, X. Gai, L. Brilland, D. Méchin, C. Caillaud, J. Troles, B. Luther-Davies, and O. Bang, "Multi-milliwatt mid-infrared supercontinuum generation in a suspended core chalcogenide fiber," Opt. Express **23**(3), 3282–3291 (2015).
7. B. Wu, Z. Zhao, X. Wang, Y. Tian, N. Mi, P. Chen, Z. Xue, Z. Liu, P. Zhang, and X. Shen, *et al.*, "Mid-infrared supercontinuum generation in a suspended-core tellurium-based chalcogenide fiber," Opt. Mater. Express **8**(5), 1341–1348 (2018).
8. O. Mouawad, J. Picot-Clémente, F. Amrani, C. Strutynski, J. Fatome, B. Kibler, F. Désévédavy, G. Gadret, J.-C. Jules, D. Deng, Y. Ohishi, and F. Smektala, "Multioctave midinfrared supercontinuum generation in suspended-core chalcogenide fibers," Opt. Lett. **39**(9), 2684–2687 (2014).
9. H. Ebendorff-Heidepriem and T. M. Monro, "Extrusion of complex preforms for microstructured optical fibers," Opt. Express **15**(23), 15086–15092 (2007).
10. X. Han, C. You, S. Dai, P. Zhang, Y. Wang, F. Guo, D. Xu, B. Luo, P. Xu, and X. Wang, "Mid-infrared supercontinuum generation in a three-hole $Ge_{20}Sb_{15}Se_{65}$ chalcogenide suspended-core fiber," Opt. Fiber Technol. **34**, 74–79 (2017).
11. H. El Hamzaoui, L. Bigot, G. Bouwmans, I. Razdobreev, M. Bouazaoui, and B. Capoen, "From molecular precursors in solution to microstructured optical fiber: a sol-gel polymeric route," Opt. Mater. Express **1**(2), 234–242 (2011).
12. J. Lægsgaard and A. Bjarklev, "Microstructured optical fibers- fundamentals and applications," J. Am. Ceram. Soc. **89**(1), 2–12 (2006).
13. A. Fitt, K. Furusawa, T. Monro, C. Please, and D. Richardson, "The mathematical modelling of capillary drawing for holey fibre manufacture," J. Eng. Math. **43**(2/4), 201–227 (2002).
14. G. Luzi, P. Epple, C. Rauh, and A. Delgado, "Study of the effects of inner pressure and surface tension on the fibre drawing process with the aid of an analytical asymptotic fibre drawing model and the numerical solution of the full N.-St. equations," Arch. Appl. Mech. **83**(11), 1607–1636 (2013).
15. C. J. Voyce, A. D. Fitt, J. R. Hayes, and T. M. Monro, "Mathematical modeling of the self-pressurizing mechanism for microstructured fiber drawing," J. Lightwave Technol. **27**(7), 871–878 (2009).
16. R. M. Wynne, "A fabrication process for microstructured optical fibers," J. Lightwave Technol. **24**(11), 4304–4313 (2006).
17. R. Kostecki, H. Ebendorff-Heidepriem, S. C. Warren-Smith, and T. M. Monro, "Predicting the drawing conditions for microstructured optical fiber fabrication," Opt. Mater. Express **4**(1), 29–40 (2014).

Optical Materials EXPRESS

18. Y. Stokes, P. Buchak, D. Crowdy, and H. Ebendorff-Heidepriem, "Drawing of micro-structured fibres: circular and non-circular tubes," J. Fluid Mech. **755**, 176–203 (2014).
19. M. J. Chen, Y. M. Stokes, P. Buchak, D. G. Crowdy, H. T. Foo, A. Dowler, and H. Ebendorff-Heidepriem, "Drawing tubular fibres: experiments versus mathematical modelling," Opt. Mater. Express **6**(1), 166–180 (2016).
20. Y. Chen and T. A. Birks, "Predicting hole sizes after fibre drawing without knowing the viscosity," Opt. Mater. Express **3**(3), 346–356 (2013).
21. http://www.irradianceglass.com/.
22. H. Ebendorff-Heidepriem and T. M. Monro, "Analysis of glass flow during extrusion of optical fiber preforms," Opt. Mater. Express **2**(3), 304–320 (2012).
23. https://www.vitron.de/english/IR-Glaeser/Kurzvorstellung.php.
24. K. Boyd, H. Ebendorff-Heidepriem, T. M. Monro, and J. Munch, "Surface tension and viscosity measurement of optical glasses using a scanning CO_2 laser," Opt. Mater. Express **2**(8), 1101–1110 (2012).
25. N. Parikh, "Effect of atmosphere on surface tension of glass," J. Am. Ceram. Soc. **41**(1), 18–22 (1958).
26. H. Parnell, D. Furniss, Z. Tang, N. C. Neate, T. M. Benson, and A. B. Seddon, "Compositional dependence of crystallization in Ge-Sb-Se glasses relevant to optical fiber making," J. Am. Ceram. Soc. **101**(1), 208–219 (2017).
27. W. Wei, L. Fang, X. Shen, and R. Wang, "Crystallization kinetics and thermal stability in Ge-Sb-Se glasses," Phys. Status Solidi B **250**(1), 59–64 (2013).
28. S. Martinková, J. Bartá, P. Koštál, J. Malek, and H. Segawa, "Extended study on crystal growth and viscosity in Ge-Sb-Se bulk glasses and thin films," J. Phys. Chem. B **121**(33), 7978–7986 (2017).
29. S. Wu, S. Fleming, B. T. Kuhlmey, J. G. Hayashi, H. Ebendorff-Heidepriem, and A. Stefani, "Stack-and-draw microstructured optical fiber with $Ge_{28}Sb_{12}Se_{60}$ chalcogenide glass," in *Advanced Photonics 2018 (BGPP, IPR, NP, NOMA, Sensors, Networks, SPPCom, SOF)*, (Optical Society of America, 2018), p. JTu5A.69.
30. https://sydney.edu.au/science/physics/cudos/research/mofsoftware.shtml.